

Direct measurement of the dependence of the photon-number distribution on the number of modes in parametric down-conversion

L. Dovrat, M. Bakstein, D. Istrati, A. Shaham and H. S. Eisenberg

Racah Institute of Physics, Hebrew University of Jerusalem, Israel

hagai.eisenberg@huji.ac.il

Abstract: Optical parametric down-conversion (PDC) is a central tool in quantum optics experiments. The number of collected down-converted modes greatly affects the quality of the produced photon state. We use Silicon Photomultiplier (SiPM) number-resolving detectors in order to directly observe the photon-number distribution of a PDC source, and show its dependence on the number of collected modes. Additionally, we show how the stimulated emission of photons and the partition of photons into several modes determine the overall photon number. We present a novel analytical model for the optical crosstalk effect in SiPM detectors, and use it to analyze the results.

© 2019 Optical Society of America

OCIS codes: (270.0270) Quantum optics, (270.5290) Photon statistics, (190.4975) Parametric processes

References and links

1. L. Mandel and E. Wolf, *Optical Coherence and Quantum Optics* (Cambridge University Press, 1995).
2. P. G. Kwiat, K. Mattle, H. Weinfurter, A. Zeilinger, A. V. Sergienko, and Y. Shih, "New high-intensity source of polarization-entangled photon pairs," *Phys. Rev. Lett.* **75**, 4337–4341 (1995).
3. E. Waks, E. Diamanti, B. C. Sanders, S. D. Bartlett, and Y. Yamamoto, "Direct observation of nonclassical photon statistics in parametric down-conversion," *Phys. Rev. Lett.* **92**, 113602 (2004).
4. E. Waks, B. C. Sanders, E. Diamanti, and Y. Yamamoto, "Highly nonclassical photon statistics in parametric down-conversion," *Phys. Rev. A* **73**, 033814 (2006).
5. O. A. Ivanova, T. S. Iskhakov, A. N. Penin, and M. V. Chekhova, "Multiphoton correlations in parametric down-conversion and their measurement in the pulsed regime," *Quantum Electronics* **36**, 951 (2006).
6. C. T. Lee, "Nonclassical photon statistics of two-mode squeezed states," *Phys. Rev. A* **42**, 1608–1616 (1990).
7. H. S. Eisenberg, G. Khoury, G. A. Durkin, C. Simon, and D. Bouwmeester, "Quantum entanglement of a large number of photons," *Phys. Rev. Lett.* **93**, 193901 (2004).
8. D. Lincoln, "A large statistics study of the performance and yields of generation-6 vlpes (histe-vi)," *Nuclear Instruments and Methods in Physics Research Section A: Accelerators, Spectrometers, Detectors and Associated Equipment* **453**, 177 – 181 (2000).
9. D. Achilles, C. Silberhorn, C. Sliwa, K. Banaszek, I. A. Walmsley, M. J. Fitch, B. C. Jacobs, T. B. Pittman, and J. D. Franson, "Photon-number-resolving detection using time-multiplexing," *Journal of Modern Optics* **51**, 1499–1515 (2004).
10. D. Rosenberg, A. E. Lita, A. J. Miller, and S. W. Nam, "Noise-free high-efficiency photon-number-resolving detectors," *Phys. Rev. A* **71**, 061803 (2005).
11. B. E. Kardynal, Z. Yuan, and A. J. Shields, "An avalanche photodiode-based photon-number-resolving detector," *Nat. Photonics* **2**, 425 (2008).
12. E. Dauler, A. Kerman, B. Robinson, J. Yang, B. Voronov, G. Goltsman, S. A. Hamilton, and K. Berggren, "Photon-number-resolution with sub-30-ps timing using multi-element superconducting nanowire single photon detectors," *J. Mod. Opt.* **56**, 365 (2009).

13. P. Kok, H. Lee, and J. P. Dowling, "Creation of large-photon-number path entanglement conditioned on photodetection," *Phys. Rev. A* **65**, 052104 (2002).
14. Y. Gao, P. M. Anisimov, C. F. Wildfeuer, J. Luine, H. Lee, and J. P. Dowling, "Super-resolution at the shot-noise limit with coherent states and photon-number-resolving detectors," *J. Opt. Soc. Am. B* **27**, A170–A174 (2010).
15. H. S. Eisenberg, J. F. Hodelin, G. Khouri, and D. Bouwmeester, "Multiphoton path entanglement by nonlocal bunching," *Phys. Rev. Lett.* **94**, 090502 (2005).
16. R. Okamoto, J. L. O'Brien, H. F. Hofmann, T. Nagata, K. Sasaki, and S. Takeuchi, "An entanglement filter," *Science* **323**, 483–485 (2009).
17. E. Knill, R. Laflamme, and G. Milburn, "A scheme for efficient quantum computation with linear optics," *Nature* **409**, 46 (2001).
18. T. B. Pittman, B. C. Jacobs, and J. D. Franson, "Demonstration of nondeterministic quantum logic operations using linear optical elements," *Phys. Rev. Lett.* **88**, 257902 (2002).
19. G. A. Durkin, C. Simon, and D. Bouwmeester, "Multiphoton entanglement concentration and quantum cryptography," *Phys. Rev. Lett.* **88**, 187902 (2002).
20. L. Mandel, "Fluctuations of photon beams: The distribution of the photo-electrons," *Proceedings of the Physical Society* **74**, 233 (1959).
21. F. Palleari, A. Andreoni, G. Zambra, and M. Bondani, "Thermal photon statistics in spontaneous parametric downconversion," *Opt. Express* **12**, 2816–2824 (2004).
22. M. Avenhaus, H. B. Coldenstrodt-Ronge, K. Laipo, W. Mauerer, I. A. Walmsley, and C. Silberhorn, "Photon number statistics of multimode parametric down-conversion," *Phys. Rev. Lett.* **101**, 053601 (2008).
23. M. Vasilyev, S.-K. Choi, P. Kumar, and G. M. D'Ariano, "Investigation of the photon statistics of parametric fluorescence in a traveling-wave parametric amplifier by means of self-homodyne tomography," *Opt. Lett.* **23**, 1393–1395 (1998).
24. G. Bondarenko, B. Dolgoshein, V. Golovin, A. Ilyin, R. Klanner, and E. Popova, "Limited geiger-mode silicon photodiode with very high gain," *Nucl. Phys. B. (Proc. Suppl.)* **61**, 347 (1998).
25. P. Buzhan, B. Dolgoshein, L. Filatov, A. Ilyin, V. Kaplin, A. Karakash, S. Klemin, R. Mirzoyan, A. Otte, E. Popova, V. Sosnovtsev, and M. Teshima, "Large area silicon photomultipliers: Performance and appli," *Nucl. Instr. and Meth. A* **567**, 78 (2006).
26. L. Dovrat, M. Bakstein, D. Istrati, and H. Eisenberg, "Simulations of the detection process in sipm detectors," *arXiv:1109.0698v1* (2011).
27. I. Afek, A. Natan, O. Ambar, and Y. Silberberg, "Quantum state measurements using multipixel photon detectors," *Phys. Rev. A* **79**, 043830 (2009).
28. M. Akiba, K. Tsujino, K. Sato, and M. Sasaki, "Multipixel silicon avalanche photodiode with ultralow dark count rate at liquid nitrogen temperature," *Opt. Express* **17**, 16885–16897 (2009).
29. P. Eraerts, M. Legré, A. Rochas, H. Zbinden, and N. Gisin, "Sipm for fast photon-counting and multiphoton detection," *Opt. Express* **15**, 14539–14549 (2007).
30. A. Yariv, *Optical Electronics in Modern Communications* (Oxford University Press, 1991).
31. H. Lee, U. Yurtsever, P. Kok, G. M. Hockney, C. Adami, S. L. Braunstein, and J. P. Dowling, "Towards photo-statistics from photon-number discriminating detectors," *Journal of Modern Optics* **51**, 1517–1528 (2004).
32. P. Kok and S. L. Braunstein, "Postselected versus nonpostselected quantum teleportation using parametric down-conversion," *Phys. Rev. A* **61**, 042304 (2000).

1. Introduction

For more than two decades, the optical process of parametric down-conversion (PDC) [1] has been the primary photon source in quantum optics experiments [2]. This nonlinear process converts single photons into pairs of signal and idler photons, which possess quantum correlations between their various degrees of freedom. The statistical nature of this process is a subject of great interest, as the photon-number statistics of the process provide a direct indication of its non-classicality [3–6]. Additionally, the photon statistics have practical implications on state preparation schemes, where the quality of the produced state depends on the number of photons generated simultaneously within the PDC process [7].

Recent developments in photon-number resolving detectors [8–12] enable the implementation of a wide range of applications in quantum optics, including state preparation schemes [13–15], quantum state filtering [16] and quantum gates [17, 18]. Number discriminating capabilities have also been shown to aid in probing eavesdropping attacks on quantum cryptography protocols [19]. Furthermore, one of the most prominent advantages of number-resolving detectors is the ability to directly measure the photon-number statistics of an optical state.

The photon-number distribution of a PDC source can range between a thermal distribution, when a single down-converted mode is collected, and a Poisson distribution when an infinitely large number of spatial and spectral modes (multimode) is collected [20]. The photon statistics of PDC sources has been directly measured in several works [3, 4, 21, 22], all of which report a Poisson distribution. However, the majority of quantum optics schemes take great care to ascertain that only a single mode is collected. Using an indirect homodyne detection method, a thermal distribution from a parametric amplifier was demonstrated [23]. In this work, we use a photon-number resolving detector in order to directly measure the photon statistics of the signal and idler photons collected from a controlled number of modes, allowing us to observe the range of distributions between the single-mode and the multimode extremes.

The photon-number resolving detector used in this work is the Silicon Photomultiplier (SiPM) [24]. The SiPM detector is composed of multiple avalanche-photo-diodes (APD) operating in Geiger-mode, combined on a single substrate. When a photon impinges on a APD element, an electric discharge can be generated. The photons impinging on the detector are distributed across its many elements. The output signals generated by all APDs are combined to form a single output pulse whose intensity is proportional to the number of impinging photons. The SiPM detector offers a good photon-number resolution, easy integration in optical setups and operation at room temperature.

The photon statistics measured by SiPM detectors may deviate from that of the original state. The three main reasons for these deviations are: 1) the non-perfect overall photon detection efficiency (loss), which is determined by the detection and coupling efficiencies, 2) false detections caused by thermal excitations (dark counts), and 3) optical crosstalk, in which secondary photons, created by carrier relaxation in one APD element, are detected by a neighboring element, falsely increasing the photon count [25]. The descriptions of loss and dark counts are quite straightforward. However, several currently available models for the crosstalk effect are either computationally difficult [26] or only applicable under limiting conditions [27–29]. We introduce here an analytical crosstalk model which can be applied for the entire range of experimental settings.

This paper is organized as follows: Sec. 2 describes the experimental setup for the generation of PDC states and their detection using a SiPM photon-number resolving detector. In Sec. 3 we present a model for the distortion effects in the SiPM detector, that includes a new approach to the crosstalk effect. This model is used for the interpretation of experimental data and the reconstruction of the original photon-number statistics. In Sec. 4 we present measurements of photon-number distributions of parametric down-conversion and their dependence on the number of collected modes.

2. The Experimental Setup

We have measured the photon-number distributions of the polarization modes of a stimulated type-II collinear PDC process. The experimental setup is shown in Fig. 1(a). Pulses of 150 fs at a repetition rate of 250 kHz were amplified, frequency doubled to 390 nm and used to pump a type-II collinear β – BaB₂O₄ (BBO) nonlinear crystal. The degenerate wavelength signal and idler photons at 780 nm, which are created with orthogonal polarizations (horizontal (H) and vertical (V)), are split at a polarizing beam splitter (PBS) and detected separately using two photon-number resolving detectors. This work focuses on measuring the photon-number distribution of a single polarization mode. Thus, the detection of both polarization modes is only used to evaluate the heralded detection efficiency of the SiPM detector. The results presented for a single polarization mode also apply to the photon pair statistics, as a collinear process produces the same statistics for pairs and for individual photons. Before the photons are coupled to the detectors, they are spectrally and spatially filtered by bandpass filters and by optical fibers,

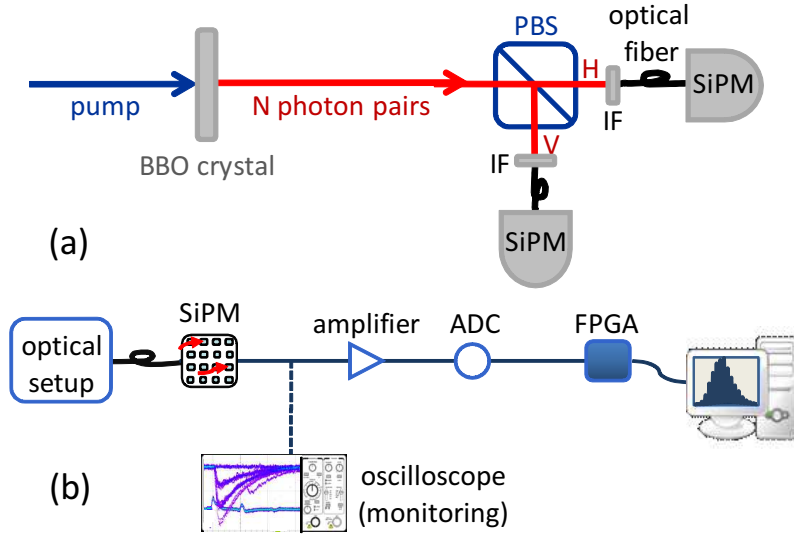


Fig. 1. (a) The experimental setup. A type-II collinear BBO crystal pumped by 390 nm amplified pulses at a repetition rate of 250 kHz. The signal and idler photons are split at a Polarizing Beam Splitter (PBS) according to their polarization and detected by two SiPM detectors. The number of spatial and spectral modes which are collected is varied using interference filters (IF) with different bandwidths and different optical fibers. (b) The detection configuration. A SiPM detector produces a signal whose intensity is proportional to the number of impinging photons. This signal is amplified, digitized using analog-to-digital converters (ADC) and analyzed using FPGA electronics in real-time. The data is continuously transmitted to a computer, which displays the photon-number distribution.

respectively. The number of spatial modes which are collected can be changed by using optical fibers with different core diameters and numerical apertures [30], and the number of collected spectral modes can be changed by using filters of different bandwidths.

The detection configuration is shown in figure 1(b). The optical signal from the photon source is coupled to a SiPM detector (*Hamamatsu Photonics, S10362-11-100U*) using optical fibers. The output electrical signal from the detector is amplified using low-noise amplifiers, digitized and then analyzed by FPGA electronics, where the number of detected photons is extracted in real time. This data is continuously transmitted to a computer, which presents the statistics. In order to minimize the effects of dark counts and after-pulsing [25], the 1 ns long sampling time of the analog electrical signal is synchronized with the arrival time of the photons. The dark counts are further reduced by moderately cooling the detectors using a thermoelectric cooler to $\approx -10^\circ\text{C}$, and the bias voltage level applied to the SiPM is modified accordingly.

3. The SiPM Detection Model

In order to interpret the measured statistics, the effects of loss, dark counts, and optical crosstalk must be properly modeled. If the measured photon-number distribution is represented by a vector of probabilities \vec{p}_m , the original probability distribution \vec{p}_o , is related to the measured distribution through the relation

$$\vec{p}_m = \mathbf{M} \cdot \vec{p}_o. \quad (1)$$

Each component of the distortion matrix \mathbf{M} is the conditional probability $M_{nm} \equiv M(n|m)$ of measuring n photons given that m original photons arrived at the detector. Using Eq. 1, the

original distribution can be reconstructed, in principle, by multiplying the measured distribution with the inverse of the distortion matrix. This method, however, is limited to relatively large probabilities and may produce non-physical results otherwise [31]. Another approach, which we use here, is to apply a fitting algorithm which finds the original distribution based on a goodness of fit test.

The matrix \mathbf{M} can be written as a product of three matrices, $\mathbf{M} = \mathbf{M}_{ct} \cdot \mathbf{M}_{loss} \cdot \mathbf{M}_{dk}$, which represent the crosstalk (ct), loss and dark counts (dk) effects. The individual matrices are constructed as follows:

Dark counts

The probability of dark counts is assumed to follow a Poisson distribution [31] of the form

$$\mathbf{M}_{dk}(n|m) = \begin{cases} 0 & n < m \\ \frac{\lambda_{dk}^{-(n-m)} \exp(-\lambda_{dk})}{(n-m)!} & n \geq m, \end{cases} \quad (2)$$

where λ_{dk} is the average number of dark counts.

Loss

The probability for loss is described by the relation [31]

$$\mathbf{M}_{loss}(n|m) = \begin{cases} \binom{m}{n} \eta^n (1-\eta)^{m-n} & n \leq m \\ 0 & n > m, \end{cases} \quad (3)$$

where η is the overall detection efficiency.

Crosstalk

Optical crosstalk occurs when a secondary photon generated during an electronic discharge in one APD element is detected in a neighboring APD element, thereby creating a secondary avalanche. Photons produced in the secondary avalanches can then continue to trigger further avalanches in additional elements (crosstalk-generated-crosstalk). The crosstalk probabilities in our model are calculated by dividing the crosstalk events into stages and recursively counting the number of possible crosstalk events in each stage. The recursion formula for the crosstalk matrix element is:

$$\mathbf{M}_{ct}(n|m) = \begin{cases} \sum_{n_{ct}=0}^{\min(m,n-m)} \binom{m}{n_{ct}} \cdot \varepsilon^{n_{ct}} (1-\varepsilon)^{m-n_{ct}} \cdot \mathbf{M}_{ct}(n-m|n_{ct}) & n \geq m > 0 \\ 1 & n = m = 0 \\ 0 & \text{otherwise,} \end{cases} \quad (4)$$

where ε is defined as the overall probability for a crosstalk-avalanche to be generated in any of the four neighboring elements. Each stage has m triggered elements which can trigger up to m new crosstalk events. The probability of generating n_{ct} new crosstalk events is composed of the probability that n_{ct} elements out of the m possible will generate crosstalk, while the remaining $m - n_{ct}$ elements will not. This probability also includes the combinatorial factor of choosing the n_{ct} crosstalk-generating elements out of the possible m . The n_{ct} crosstalk-triggered elements continue to generate additional crosstalk events in a recursive way, until all of the $n - m$ crosstalk elements are triggered.

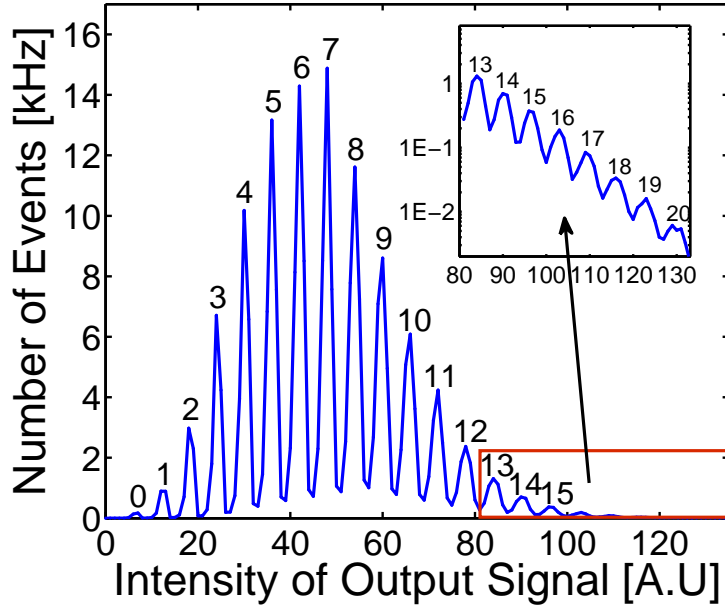


Fig. 2. A histogram of the electrical output signal level for a coherent input state. The data was accumulated over a period of 30 seconds. Good peak separation is maintained up to 20 photons.

This novel analytical crosstalk model does not limit the number of crosstalk events and also accounts for crosstalk-generated-crosstalk. The model was developed since other available analytical models [27–29] were inconsistent with our experimental results due to limitations on the crosstalk probability values and the number of crosstalk events. Our model does not account for the geometrical arrangement of the APD elements in the detector, nor its finite size. However, we show below that for values within the experimental range, this analytical model agrees with a numerical model that has no such limitations [26]. Additionally, this model is less computationally demanding than the numerical model. Thus, it is a useful tool in the interpretation of experimental data from photon-number resolving detectors, where crosstalk between the detection elements plays a crucial role.

4. Results and Discussion

Figure 2 shows an example of a histogram of pulse intensities produced by a coherent state. The probability of detecting n photons is proportional to the area of the n^{th} Gaussian. We obtain high photon-number discrimination for as high as 20 photons. The number of resolvable photons is limited due to the decrease of the signal to noise ratio as the number of photons is increased.

We demonstrate the use of our model for reconstructing the original photon statistics with the photon-number distribution measurements of a thermal state. The original thermal distribution can be written as

$$p_{th}(n) = \frac{1}{(1 + \bar{n}) (1 + \frac{1}{\bar{n}})^n}, \quad (5)$$

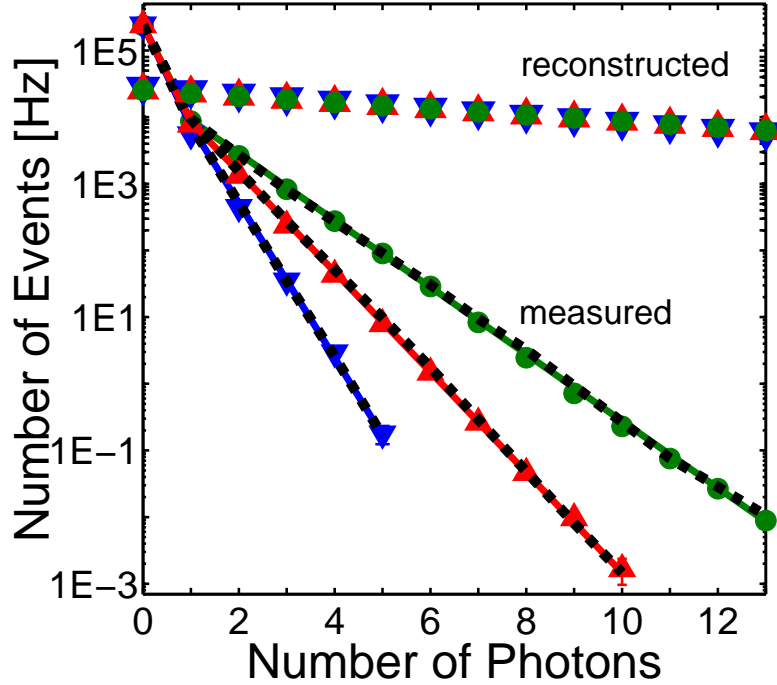


Fig. 3. Measurements of a thermal state conducted on a polarization mode of a type-II collinear PDC source, spatially and spectrally filtered using a single-mode fiber and a 3 nm bandpass filter. The experimental data was fitted to the obtained statistics using the model presented in this work (solid lines). The reconstruction of the original photon statistics from the measured data is also shown. The data was obtained at a temperature of -10°C for bias voltages of (a) $V_{bias} = 68.3\text{ V}$, (b) $V_{bias} = 67.7\text{ V}$, and (c) $V_{bias} = 67.4\text{ V}$. The fit parameters were (a) $\eta = 0.006 \pm 0.001$, $\lambda_{dk} = 0.4 \pm 0.1$, $\bar{n} = 8.9 \pm 0.5$, $\varepsilon = 0.280 \pm 0.005$ (green circles) (b) $\eta = 0.0049 \pm 0.0003$, $\lambda_{dk} = 0.21 \pm 0.06$, $\bar{n} = 8.8 \pm 0.5$, $\varepsilon = 0.140 \pm 0.006$ (red upward triangles) (c) $\eta = 0.0042 \pm 0.0005$, $\lambda_{dk} = 0.06 \pm 0.03$, $\bar{n} = 7.8 \pm 2.7$, $\varepsilon = 0.040 \pm 0.006$ (blue downward triangles). The corresponding crosstalk values obtained with the numerical model of Ref. [26] are (a) $\varepsilon_{nn} = 0.078 \pm 0.001$, (b) $\varepsilon_{nm} = 0.038 \pm 0.001$ (c) $\varepsilon_{nn} = 0.010 \pm 0.001$. Fits using the numerical model are presented by black dashed lines.

where \bar{n} is the average number of photons. The measured distribution exhibits a lower value of \bar{n} due to losses and deviates from the power-law dependence of Eq. 5 due to optical crosstalk and dark counts. We measured the same thermal state with three different sets of values for the amount of loss, dark counts and crosstalk, obtained by operating the SiPM detector with different bias voltage values [25]. As a result, we obtained three different measured distributions, although the original photon-number distribution was the same. The measurements are shown in Fig. 3. The main distortions in the distributions are the low values of \bar{n} due to losses and the deviation from a straight line in the semi-log plot when the number of measured photons exceeds 1. The latter is the effect of the crosstalk process, which falsely increases the probability of measuring high numbers of photons. The crosstalk probabilities of these measurements range from the highest probability value (maximum bias voltage), which creates the highest deviation, to the minimal probability (minimal bias voltage) which creates the lowest deviation.

The original distribution is reconstructed by fitting the measured data \vec{p}_m to the function

$\vec{p}_m = M_{ct} M_{loss} M_{dk} \vec{p}_{th}$, where \vec{p}_{th} is the thermal distribution of Eq. 5 and \bar{n} is the only free parameter. The overall detection efficiency η , the average number of dark counts λ_{dk} , and the crosstalk probability ε , that are used for the construction of the distortion matrices, are measured separately. The value of η is defined as the heralded efficiency between the two down-converted polarization modes and is determined by the ratio between two-photon coincidence and single-photon counts in the limit $\bar{n} \ll 1$. The dark counts and crosstalk parameters are obtained through a separate measurement of the Poissonian dark count statistics which are fit to the function $\vec{p}_m = M_{ct} M_{loss} M_{dk} \vec{1}$, where $\vec{1}$ is a vector of zeros with 1 at the first position, and λ_{dk} and ε are the free fit parameters.

All three measurements in Fig. 3 were reconstructed to the same original state, within the margins of error, despite the different measured distributions. This result indicates the consistency of our evaluation of the dark counts, loss and crosstalk parameters. We compare these results to those obtained using the numerical crosstalk model introduced in Ref. [26]. The numerical model is based on simulations of the detection process, and takes into account the geometrical configuration of the detector, the finite number of detection elements, and possible attempts to trigger neighboring cells which have already been triggered. The model is characterized through a parameter ε_{nn} , defined as the probability of generating crosstalk in one particular neighbor among the four nearest neighbors, rather than the overall probability of generating crosstalk among the nearest neighbors, which we define here as ε . The values of ε_{nn} obtained from the fit correspond to the values of ε through the relation $\varepsilon = 1 - (1 - \varepsilon_{nn})^4$ [26]. The agreement between the two models shows that although the analytical model does not account for the geometry of the detector, it provides a good description of the crosstalk process for all crosstalk values in the experimental range.

We now consider the photon-number distributions of down-converted photons as a function of the number of collected modes. If n photons are distributed among s modes, such that $n_1 + n_2 + \dots + n_s = n$, then the overall probability of measuring n photons is given by [20]:

$$p_s(n) = \binom{s+n-1}{s-1} \cdot \prod_{i=1}^s p(n_i), \quad (6)$$

where the product $\prod_{i=1}^s p(n_i)$ is the joint probability of measuring n_i photons in each mode i , and the combinatorial factor amounts to the number of possible arrangements of n indistinguishable photons into s modes. If the photons are distributed evenly among the modes, the average number of photons in each mode is uniform and equals $\bar{n}_i = \bar{n}/s$. The photon-number distribution within each of the modes is thermal, $p(n_i) \equiv p_{th}(n_i)$, and by substituting Eq. 5 into Eq. 6, we obtain the following probability distribution

$$p_s(n) = \binom{s+n-1}{s-1} \frac{1}{\left(1 + \frac{\bar{n}}{s}\right)^s \left(1 + \frac{s}{\bar{n}}\right)^n}. \quad (7)$$

This distribution converges to a Poisson distribution when the number of modes approaches infinity.

The dependence of the photon-number distribution on the number of modes is demonstrated by measuring the photon statistics collected from a controlled number of modes. Figure 4 shows four representative measurements of the photon-number distributions which range between a single mode (thermal) distribution, and a multimode (Poisson) distribution. The solid lines are fits to the function $\vec{p}_m = M_{ct} M_{loss} M_{dk} \vec{p}_s$, where \vec{p}_s is defined in Eq. 7 with \bar{n} and s as the free parameters. We detected up to 14 photons and obtained good fits to the data. The inset in Fig. 4 shows a close-up of one of the distributions along with the corresponding theoretical single-mode and multimode distributions for the same fit parameters. Notice that the difference

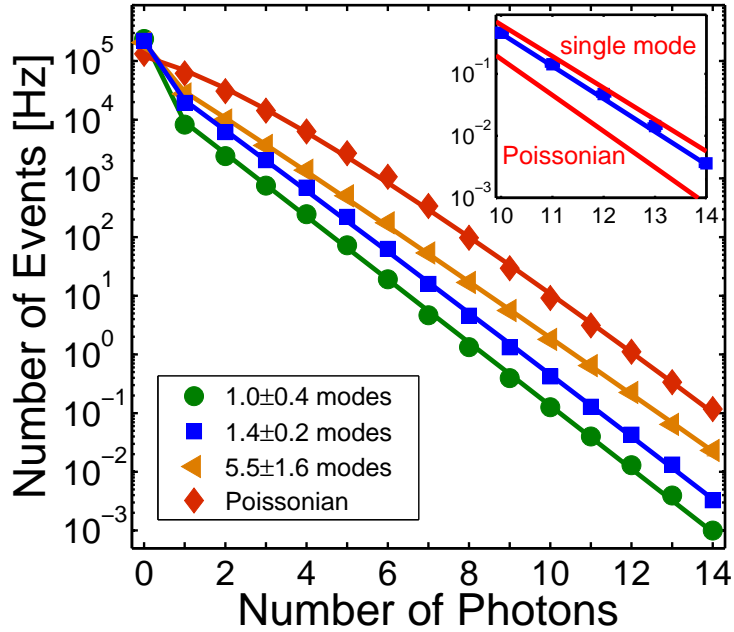


Fig. 4. Representative photon-number distribution measurements and their fits. The results are presented for distributions which range between thermal and Poissonian statistics. Experimental errors are smaller than their respective symbol size. The inset shows the measurement with 1.4 modes (blue squares) plotted with the corresponding single-mode and Poisson distributions for the same average number of photons. The measurements were taken with the following parameters: (a) $\eta = 0.013$, $\lambda_{dk} = 0.15$, $\varepsilon = 0.26$, 3 nm bandwidth filter, single mode fiber for 780 nm, integration time of 780 minutes (green circles) (b) $\eta = 0.019$, $\lambda_{dk} = 0.11$, $\varepsilon = 0.23$, 3 nm bandwidth filter, single mode fiber for 1500 nm, integration time of 100 minutes (blue squares) (c) $\eta = 0.013$, $\lambda_{dk} = 0.13$, $\varepsilon = 0.27$, 10 nm bandwidth filter, single mode fiber for 1500 nm, integration time of 100 minutes (orange triangles) (d) $\eta = 0.020$, $\lambda_{dk} = 0.15$, $\varepsilon = 0.22$, 3 nm bandwidth filter, multimode fiber for 780 nm, integration time of 115 minutes (red diamonds)

between the distributions becomes more marked as the number of photons increases. The difference is almost undetectable for low photon numbers. In fact, measurements of at least 10 photons are required for our experimental parameter range, in order to properly discriminate between distributions with different mode numbers.

The number of modes obtained for all combinations of fibers and filters is shown in table 1. The non-integer mode numbers should be interpreted as a weighted number of occupied modes and result from a non-uniform distribution of photons between the modes. We can discriminate between distributions containing up to about 10 modes, as distributions containing over 10 modes cannot be distinguished from Poisson distributions. Table 1 shows the proportional increase of the number of spectral modes with the increase in the bandwidth of the bandpass filters. The width of the phase-matched spectrum of the down-converted photons is estimated to be ≈ 10 nm. The number of spatial modes measured with our system is also consistent with the choice of fibers. When the PDC photons, which passed through a 3 nm bandpass filter, were coupled into a single mode fiber for 780 nm, a thermal distribution was produced. Whereas,

Table 1. The number of modes as obtained from the photon-number statistics. The table shows the number of modes for interference filters with different bandwidths and for optical fibers with different mode field diameters (MFD) and numerical apertures (NA). Measurements in the first row were taken with a single-mode fiber for 780 nm, the second row with a single-mode fiber for 1550 nm and the third row with a standard graded-index multimode fiber. Distributions are considered Poissonian for $s > 10$.

fiber type		filter bandwidth			
MFD	NA	3 nm	5 nm	10 nm	no filter
5.0 μm	0.13	1.0 \pm 0.4	1.6 \pm 0.7	2.6 \pm 1.6	3.3 \pm 1.7
10.4 μm	0.14	1.43 \pm 0.24	2.13 \pm 0.7	5.5 \pm 1.6	5.4 \pm 3.2
62.5 μm	0.275	Poissonian	—	—	—

when the photons were coupled into a multimode fiber, a Poisson distribution was produced, even though the same filter was used. The relatively small number of modes obtained with the single-mode fiber for 1550 nm can be attributed to non-uniform mode coupling, which does not equally stimulate all of the modes in the fiber.

The average number of down-converted photons in a single mode is determined by the stimulation parameter τ_i , which has a linear dependence on the pump field, the crystal length and the nonlinear coefficient of the crystal [32]. Assuming an equal distribution of the photons between s modes, the mean number of photons \bar{n} is given by

$$\begin{aligned}\bar{n} &= s \cdot \bar{n}_i \\ &= s \cdot \sinh^2(\tau_i) \\ &= s \cdot \sinh^2(\alpha \sqrt{I}),\end{aligned}\tag{8}$$

where \bar{n}_i is the average number of photons in each of the individual modes, α is the coupling constant between the pump field and the nonlinear crystal, and I is the pump intensity.

In order to show the dependence of \bar{n} on the number of modes, we measured photon-number distributions as a function of the pump intensity for the different numbers of collected modes. The values of \bar{n} were extracted by fitting the different distributions to Eq. 7. The fit values of \bar{n} as a function of the total pump power are shown in Fig. 5. All measurements show a nonlinear dependence, indicative of a stimulated process. The number of modes s obtained from these fits corresponds well to the number of modes obtained through fits to the photon-number distributions (see Fig. 4). Furthermore, all fits resulted in similar values of the α parameter, in agreement with the model of Eq. 8.

5. Conclusions

In conclusion, we have built a detection setup, which incorporates a Silicon Photomultiplier (SiPM) as a photon-number resolving detector. Our setup enables good photon-number discrimination for as many as 20 photons. The output signal of the SiPM is analyzed in real time using FPGA electronics. The measured photon-number distribution probabilities are interpreted by modeling the effects of loss, dark counts and optical crosstalk, which distort the original photon-number probabilities. We present a useful analytical crosstalk model that is applicable for all crosstalk probability values in the experimental range and includes crosstalk-generated crosstalk.

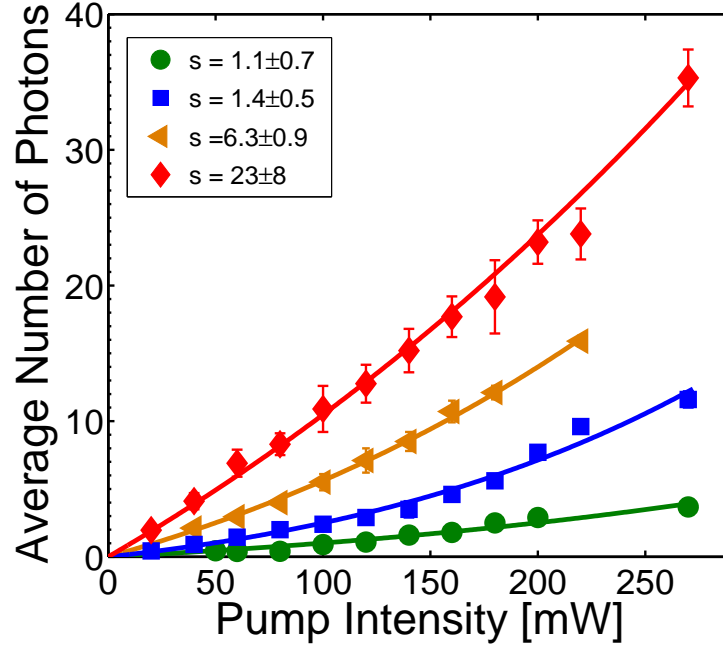


Fig. 5. The average number of photons collected from multiple modes as a function of the pump intensity. The solid lines are fits to Eq. 8 with the following parameters: (a) $s = 1.1 \pm 0.7$, $\alpha = 0.08 \pm 0.02$ (green circles) (b) $s = 1.4 \pm 0.5$, $\alpha = 0.10 \pm 0.02$ (blue squares) (c) $s = 6.3 \pm 0.9$, $\alpha = 0.08 \pm 0.01$ (orange triangles). (d) $s = 23 \pm 8$, $\alpha = 0.06 \pm 0.01$ (red diamonds).

We have performed measurements of photon-number distributions of a single polarization mode of a collinear type-II PDC process. The high photon-number resolution of our system enables the differentiation between distributions collected from a different number of spectral and spatial modes. We present distributions which range from single-mode (thermal) to multimode (Poissonian) statistics. The results show how the photon-number distribution is determined by the number of collected modes. Furthermore, we show the dependence of the average number of photons on the number of collected modes, and the stimulated nature of parametric down-conversion.